Optical Realization of Double-Continuum Fano Interference and Coherent Control in Plasmonic Metasurfaces

Nihal Arju,[1] Tzuhsuan Ma,[1] Alexander Khanikaev,[2] David Purtseladze,[1] and Gennady Shvets[1,*]
[1]Department of Physics, The University of Texas at Austin, One University Station C1500, Austin, Texas 78712, USA
[2]Department of Physics, Queens College of The City University of New York, Queens, New York 11367, USA
(Received 14 August 2014; published 11 June 2015)

Classical realization of a ubiquitous quantum mechanical phenomenon of double-continuum Fano interference using metasurfaces is experimentally demonstrated by engineering the near-field interaction between two bright and one dark plasmonic modes. The competition between the bright modes, one of them effectively suppressing the Fano interference for the orthogonal light polarization, is discovered. Coherent control of optical energy concentration and light absorption by the ellipticity of the incident light is theoretically predicted.

DOI: 10.1103/PhysRevLett.114.237403 PACS numbers: 78.67.Pt, 42.25.Bs, 73.20.Mf, 81.05.Xj

Ugo Fano's breakthrough paper [1] that explained asymmetric ionization spectra in atomic systems by introducing the now eponymous interference between discrete and continuous states continues to be highly influential despite its publication more than half a century ago. Universal concepts of Fano resonance, interference, and line shape have been applied to several areas of optical science, including photonics, plasmonic nanostructures, and metamaterials [2–6]. The sharp spectral features in Fano-resonant metamaterials, combined with strong optical energy concentration, make them attractive for sensing and fingerprinting [7–10] and nonlinear [11,12] applications.

Most of the recently reviewed [4,5,13] work on optical Fano resonances deals with near-field coupling between a single bright and a single dark resonance, respectively, emulating the continuum and discrete atomic states. However, the original Fano paper addressed a much broader class of couplings between atomic states, including one discrete and multiple continuum states. The key difference between the single-continuum and double-continuum cases is that the ionization probability vanishes for at least some values of energy loss of the ionizing particle in the former but not in the latter case [1]. Thus, the magnitude of Fano interference can be suppressed by the second continuum state.

In this Letter, we report the realization of the optical analog of double-continuum Fano (DCF) interference using a circularly dichroic (CD) plasmonic metasurface shown in Fig. 1, which supports one dark and two bright plasmonic modes. The modes are controllably coupled to each other in the near field through symmetry-breaking vertical displacement s_y of a horizontal nanorod coupler (HNC) from its symmetric position. Our experimental measurements of Fano-shaped polarized reflectivity spectra $R_{xx}(\lambda)$ and $R_{yy}(\lambda)$ shown in Figs. 2(a) and 2(b) reveal a new optical phenomenon of *continuum state competition* in asymmetric photonic structures: the presence of the second (e.g., y-polarized) continuum state can significantly affect the strength of the Fano interference of the dark state with the first (e.g., x-polarized) continuum state. Unlike the plasmonic phenomenon [14] of the Fano feature reduction by *nonradiative* (Ohmic) losses, the continuum state competition directly emulates the atomic systems [1] where the nonradiative decay rate of the discrete state is naturally negligible. This phenomenon was not addressed in the

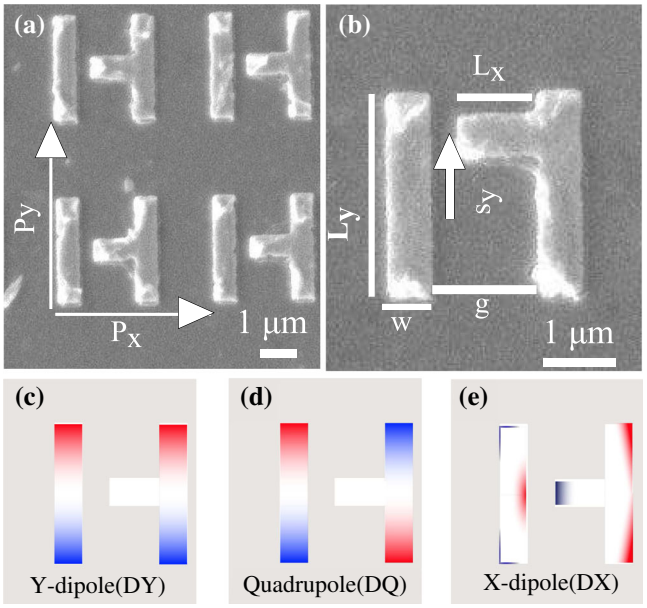

FIG. 1 (color online). (a) Scanning electron micrograph of a fabricated DCF metasurface. (b) Geometry definitions of a unit cell ($s_y = 0.52$ μm). For all metasurfaces: $P_x = 2.7$, $P_y = 3.15$, $w = 0.36$, $L_x = 0.92$, $L_y = 1.8$, and $g = 0.66$ μm. (c)–(e) Charge distributions of the three unperturbed eigenmodes of the symmetric ($s_y = 0$) metasurface. (c) and (e) Bright DY and DX, (d) dark DQ.

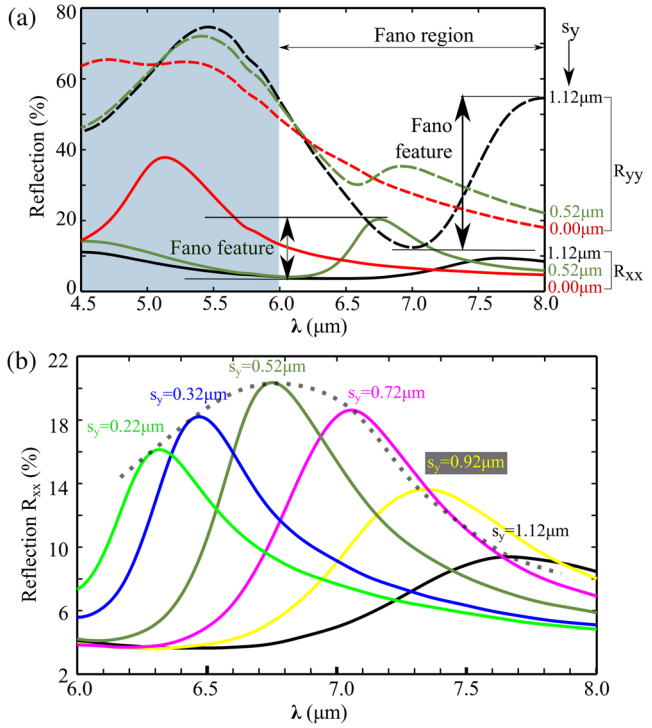

FIG. 2 (color online). (a) Measured reflectivity spectra R_{xx} (solid lines) and R_{yy} (dashed lines). Fano feature in R_{yy} is larger than in R_{xx} for $s_y = 1.12$ μm (black line); the opposite is true for $s_y = 0.52$ μm (green line). Fano features are absent for $s_y = 0$ (red lines). (b) Zoomed-in R_{xx} spectra for 0.22 μm $< s_y <$ 1.22 μm. Dotted line: nonmonotonic behavior of the Fano feature with s_y interpreted as the competition between x- and y-polarized continua.

earlier optical DCF work [15,16] because the relative mode coupling cannot be controlled in a fixed geometry structure.

An important practical implication of DCF is the possibility of controlling the intensity of light concentrated at the metasurface using the ellipticity of the incident optical beam. Specifically, we demonstrate that by simply adjusting the phase difference between the x- and y-polarized electric field components of incident light, one can vary the intensity of concentrated light by more than an order of magnitude. Such coherently controlled optical field enhancement can be utilized for sensing and nonlinear applications. Moreover, because light intensity determines its absorption, CD metasurfaces open a new path to interference-based control of single-beam absorption, which is reminiscent of two-channel coherent absorbers [17]. The consequences of such coherent absorption control include giant CD in absorption and transmission [18].

Experimental results.—A family of gold metasurfaces shown in Fig. 1 with different symmetry-breaking parameters s_y were fabricated on CaF_2 substrates using electron beam lithography. The lowest plasmonic resonances of the metasurfaces shown in Fig. 1 are classified as one dark quadrupolar (DQ) and two bright dipolar (DX and DY) plasmonic modes that are radiatively coupled to incident light polarized in the x and y directions, respectively, giving rise to two quasicontinua of electromagnetic states. The finite displacement s_y of the HNC that perturbs the DQ mode is used to control the coupling between the modes. Polarized reflection coefficients were measured using Fourier transform infrared microspectroscopy. The $R_{yy}(\lambda)$ and $R_{xx}(\lambda)$ spectra shown in Fig. 2(a) reveal broad reflectivity peaks inside the shaded (4.5 μm $< \lambda <$ 6 μm) spectral window, corresponding to the bright DY and DX resonances, respectively. In the rest of the Letter we concentrate on the 6 μm $< \lambda_{DQ}(s_y) <$ 8 μm spectral window containing the dark DQ mode.

Several key observations can be made based on the spectral Fano features measured for a wide range of the symmetry-breaking parameter s_y. First, we conclude from Fig. 2(a) that the relative coupling strengths $\tilde{\kappa}_{XQ}(s_y)$ (between DQ and DX) and $\tilde{\kappa}_{YQ}(s_y)$ (between DQ and DY) vary widely with s_y. This conjecture follows from the very different manifestations of Fano resonance in R_{xx} and R_{yy} spectra. Specifically, for small values of $s_y < L_y/4$, the Fano feature in the x polarization becomes strongly pronounced while it is barely noticeable in y polarization (e.g., $s_y = 0.52$ μm). The opposite is true for large values of s_y: the Fano feature in $R_{yy}(\lambda)$ is much stronger than in $R_{xx}(\lambda)$ for $s_y \geq L_y/2$ (e.g., $s_y = 1.12$ μm).

Second, we observe from Fig. 2(b) that the magnitude of the Fano feature in x polarization is nonmonotonic in s_y. The peak value of R_{xx} (dotted line) plotted in Fig. 2(b) increases with s_y, reaches the maximum at $s_y \equiv s_y^{max} \approx 0.52$ μm, and decreases for $s_y > s_y^{max}$. The decrease of the Fano feature for large values of s_y is unexpected because the coupling coefficient $\tilde{\kappa}_{XQ}(s_y)$ continues monotonically increasing with s_y even for $s_y > s_y^{max}$. The observed decrease is the direct experimental evidence of continuum state competition in DCF originally predicted by Fano [1] for atomic systems. Specifically, the linewidth $\delta\lambda_{DQ}(s_y)$ of the radiatively broadened Fano resonance increases [and the corresponding quality factor $Q(s_y) = \lambda_{DQ}/(\delta\lambda_{DQ})$ decreases] faster with s_y than the coupling coefficient $\tilde{\kappa}_{XQ}(s_y)$, thereby suppressing the Fano feature in R_{xx}.

Theoretical model of DCF in plasmonic metasurfaces.—To explain these experimental results and to explore the possibility of circularly dichroic optical field concentration, in what follows we develop a simple analytic model of optical DCF. The interaction of light with the three modes (two quasicontinuum and one discrete) of the metasurface is described by the following equations based on the [19,20] coupled mode theory (CMT):

$$\frac{dD_Y}{dt} = i\tilde{\omega}_Y D_Y + i\kappa_{XY} D_X + \alpha_y E_y^{in},$$
$$\frac{dD_Q}{dt} = i\tilde{\omega}_Q D_Q + i\kappa_{XQ} D_X,$$
$$\frac{dD_X}{dt} = i\tilde{\omega}_X D_X + i\kappa_{XY} D_Y + i\kappa_{XQ} D_Q + \alpha_x E_x^{in}, \quad (1)$$

where D_X, D_Y, and D_Q are the mode amplitudes, and $\alpha_{x(y)}$ are the radiative coupling efficiencies of the bright resonances to the far-field x-(y-) polarized incident waves with amplitudes $E^{\text{in}}_{x(y)}$, respectively. The three modes are characterized by their complex-valued unperturbed eigenfrequencies $\tilde{\omega}_{X,Q,Y} \equiv \omega_m - i\tau_m^{-1}$ ($m = X, Y, Q$ is the resonance's index), where ω_m and τ_m are the spectral position and unperturbed lifetime of the m'th mode, respectively.

Note that the κ_{YQ} component of the near-field coupling tensor κ_{lm} has been neglected in Eq. (1) in comparison with its $\kappa_{\text{XQ}}(s_y)$ and $\kappa_{\text{XY}}(s_y)$ components for small value of s_y. Qualitatively, κ_{lm} is proportional to the overlap integral $\vec{E}_l \cdot \vec{E}_m$ inside the region occupied by the HNC. It can be observed from Figs. 1(d)–1(f) that (a) E_x is the largest electric field component for all three modes in the said region of space, and (b) $E_x = 0$ at $y = 0$ for the DQ and DY modes. Based on these symmetry considerations (see the Supplemental Material [21] for details), $\kappa_{\text{XQ}}, \kappa_{\text{XY}} \propto s_y$, but $\kappa_{\text{YQ}} \propto s_y^2$ can be neglected for $s_y \ll L_y/4$. As demonstrated below, effective coupling between DQ and DY emerges in the second order of the perturbation theory based on Eqs. (1). The resulting indirect coupling coefficient, while also $\propto s_y^2$, is larger than the neglected direct coupling term κ_{YQ} (see the Supplemental Material [21] for detailed numerical calculations). Also, from the energy conservation [13,19,20], $1/\tau_{X,Y} = |\alpha_{x,y}|^2 + 1/\tau^{\text{Ohm}}_{X,Y}$, where $1/\tau^{\text{Ohm}}_{X,Y}$ are the intrinsic decay rates.

After solving Eq. (1) in the vicinity of the dark resonance under the small-coupling ($|\kappa_{\text{XY}}|, |\kappa_{\text{XQ}}| \ll |\omega_Q - \omega_{X,Y}|$) assumption and using the expressions for the complex-valued reflection amplitudes [13] $r_{xx(yy)} = \alpha^*_{x(y)} D_{X(Y)}/E^{\text{in}}_{x(y)}$, we obtain

$$r_{xx} = \frac{\alpha_x^2}{(\omega - \tilde{\omega}_X)} + \frac{\alpha_x^2 \tilde{\kappa}_{\text{XY}}^2}{(\omega - \tilde{\omega}_Y)} + \frac{\alpha_x^2 \tilde{\kappa}_{\text{XQ}}^2}{(\omega - \tilde{\omega}'_Q)}, \tag{2}$$

$$r_{yy} = \frac{\alpha_y^2}{(\omega - \tilde{\omega}_Y)} + \frac{\alpha_y^2 \tilde{\kappa}_{\text{XY}}^2}{(\omega - \tilde{\omega}_X)} + \frac{\alpha_y^2 \tilde{\kappa}_{\text{YQ}}^2}{(\omega - \tilde{\omega}'_Q)}, \tag{3}$$

where the normalized coupling coefficients $\tilde{\kappa}_{lm}$ between the modes are given by

$$\tilde{\kappa}_{\text{XY}} = \frac{\kappa_{\text{XY}}}{\tilde{\omega}_X - \tilde{\omega}_Y}, \qquad \tilde{\kappa}_{\text{XQ}} = \frac{\kappa_{\text{XQ}}}{\tilde{\omega}_X - \tilde{\omega}_Q}, \qquad \tilde{\kappa}_{\text{YQ}} = \tilde{\kappa}_{\text{XY}}\tilde{\kappa}_{\text{XQ}}. \tag{4}$$

The renormalized or redshifted frequency ω'_Q and the radiatively reduced lifetime τ'_Q of the DQ mode are approximated as

$$\omega'_Q \approx \omega_Q - \frac{\kappa_{\text{XQ}}^2}{(\omega_X - \omega_Q)} - \frac{\kappa_{\text{XY}}^2 \kappa_{\text{XQ}}^2}{(\omega_X - \omega_Q)^2(\omega_Y - \omega_Q)},$$
$$\frac{1}{\tau'_Q} \approx \frac{1}{\tau_Q^{\text{Ohm}}} + \kappa_{\text{XQ}}^2 \frac{\alpha_x^2}{(\omega_Q - \omega_X)^2} + \kappa_{\text{XY}}^2 \kappa_{\text{XQ}}^2 \frac{\alpha_y^2(\omega_X - \omega_Q)^2 + 2\alpha_x^2(\omega_X - \omega_Q)(\omega_Y - \omega_Q)}{(\omega_X - \omega_Q)^4(\omega_Y - \omega_Q)^2}, \tag{5}$$

where the large modal separation assumption of $|\omega_{X,Y} - \omega_Q| \gg 1/\tau_{X,Y}$ is used.

The two key features of the experimentally measured $R_{xx(yy)} \equiv |r_{xx(yy)}|^2$ reflectivity spectra can now be understood by examining the dependence of the Fano feature's magnitude $r^{\text{Fano}}_{xx(yy)}$ on s_y. It is given by the third term in the right-hand side of Eqs. (2), (3) evaluated at $\omega = \omega'_Q$:

$$r_{xx}^{\text{Fano}} \propto \frac{\alpha_x^2 s_y^2}{1/\tau_Q^{\text{Ohm}} + \beta s_y^2 + \gamma s_y^4}, \qquad r_{yy}^{\text{Fano}} \propto \frac{\alpha_y^2 s_y^4}{1/\tau_Q^{\text{Ohm}} + \beta s_y^2 + \gamma s_y^4}, \tag{6}$$

where β and γ follow from Eq. (5).

We observe that the decay rate of the DCF resonance given by the denominators of Eq. (6) can be broken up into three contributions: (a) the Ohmic (nonradiative) contribution, (b) the contribution $\propto s_y^2$ corresponding to the radiative decay into the x-polarized continuum, and (c) the contribution $\propto s_y^4$ corresponding to the radiative decay into the y-polarized continuum. Depending on the relative dominance of these three mechanisms controlled by s_y, the three respective coupling regimes can be identified as the (i) weak coupling regime ($s_y < L_y/4$), (ii) intermediate coupling regime ($L_y/4 < s_y \ll L_y/2$), and (iii) strong coupling regime ($s_y \sim L_y/2$). The transition from weak to strong coupling regimes with increasing s_y explains the decrease of the quality factor of the Fano resonance with s_y evident from Fig. 2(b). The experimentally estimated quality factors of the DQ mode drop from its Ohmic loss limited value [6] of $Q = 13$ to $Q = 7$ (strong y-polarized radiative loss) as s_y increases from $s_y = 0.22$ to $s_y = 1.12$ μm.

The slower emergence of the Fano feature in the R_{yy} spectrum compared with the R_{xx} (*first* observation) can be understood from the scaling of $r_{yy}^{\text{Fano}} \propto s_y^4$ versus $r_{xx}^{\text{Fano}} \propto s_y^2$ in the weak coupling regime. The situation changes dramatically for $s_y \geq L_y/2$ and the Fano feature in R_{yy} becomes stronger than in R_{xx} because of the $\alpha_y > \alpha_x$ relationship which is the consequence of $L_y > L_x$. The *second* observation is also explained by the nonmonotonic dependence of r_{xx}^{Fano} on s_y due to the transition to strong coupling regime, where the continuum state competition [1] in DCF is responsible for the weakening of the Fano feature in R_{xx} for large s_y.

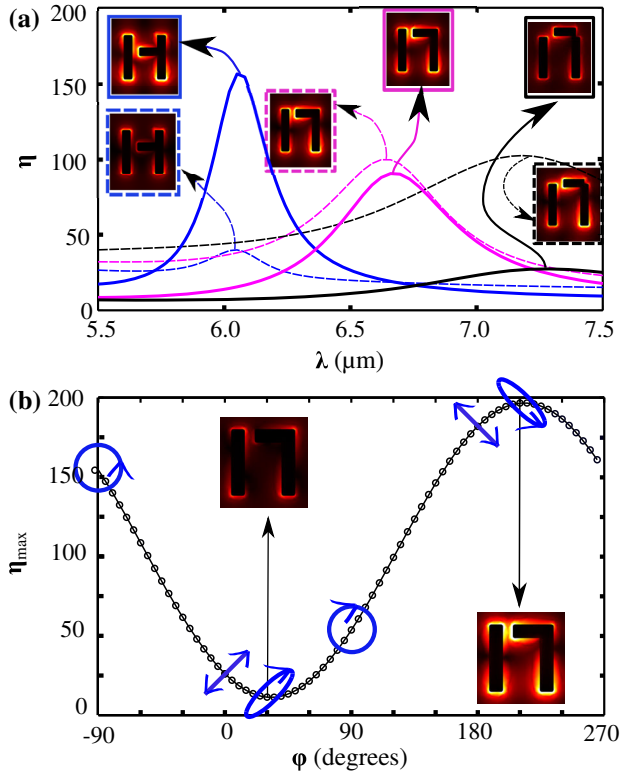

FIG. 3 (color online). COMSOL simulations of the optical intensity enhancement $\eta = \langle|\vec{E}|^2\rangle/E_0^2$ averaged over all (except metal substrate) metal interfaces in plasmonic DCF metasurfaces. (a) η for x-polarized (solid) and y-polarized (dashed lines) incident light for weak-coupled ($s_y = 0.32$ μm), intermediately coupled ($s_y = 0.72$ μm), and strongly coupled ($s_y = 1.14$ μm) regimes. Insets: near field profiles. (b) The dependence of $\eta_{\max}$ on the incident light chirality parametrized by the phase shift ϕ (see text) for the $s_y = 0.52$ μm metasurface. Insets: near-field intensities for $\phi = 30°$ (left) and $\phi = 210°$ (right). Closed directional loops indicate the polarization state of incident light as a function for $-90° < \phi < 270°$.

Circularly dichroic optical energy concentration by DCF metasurfaces.—It has been long recognized that one of the attractions of Fano-resonant structures is strong optical field enhancement due to the excitation of dark plasmonic resonances. Below we demonstrate that coherent (phase) control of optical field concentration can be accomplished through interference by engineering a general elliptic polarization state of the incident light. First, we calculate the amplitude D_Q of the dark resonance in the proximity of the DQ mode in response to the incident light with complex-valued amplitudes $(E_x, E_y) = E_0(1, \exp i\phi)/\sqrt{2}$. Here, ϕ is the relative phase between the x and y polarizations that determines the state of elliptic polarization as illustrated in Fig. 3(b). At the Fano resonance, the amplitude of the dark mode is expressed from Eq. (1) as $D_Q = (E_0/\sqrt{2})[q_{xx} + \exp(i\phi)q_{yy}]/(\omega - \tilde{\omega}'_Q)$, where

$$q_{xx} = \frac{\alpha_x \kappa_{XQ}(s_y)}{\tilde{\omega}_X - \tilde{\omega}_Q}, \qquad q_{yy} = \frac{\alpha_y \kappa_{XQ}(s_y)\kappa_{XY}(s_y)}{(\tilde{\omega}_X - \tilde{\omega}_Q)(\tilde{\omega}_Y - \tilde{\omega}_Q)} \quad (7)$$

are complex-valued field enhancement coefficients.

Because of the different scaling of q_{xx} and q_{yy} with s_y, it follows from Eq. (7) that in the weak (strong) coupling regime the strongest field enhancement is achieved for the x-(y-) polarized light. This is confirmed by electromagnetic COMSOL simulations of the surface-averaged optical intensity enhancement $\eta \equiv \langle|\vec{E}|^2\rangle/E_0^2$ shown in Fig. 3(a) for the x- and y-polarized light incident on DCF metasurfaces with different values of s_y. An even more remarkable conclusion derived from Eq. (7) is the possibility of controlling the field enhancement using elliptically polarized light.

The resulting CD (i.e., the dependence of $\eta \propto |D_Q|^2$ on ϕ) is the consequence of the finite phase difference $\Delta\phi = \arg(q_{xx}/q_{yy})$: the field enhancement is maximized (minimized) for $\phi_{\max} = \Delta\phi$ ($\phi_{\min} = \Delta\phi + \pi$) due to the constructive (destructive) interference between the two excitation pathways. Moreover, symmetry properties of the coupling coefficients κ_{XQ} and κ_{XY} ensure the following property of the structure's enantiomeric partner produced by displacing of the HNC to the opposite side ($s_y \to -s_y$) of the symmetry plane: $|D_Q|(\phi, -s_y) = |D_Q|(\phi + \pi; s_y)$.

These qualitative results are confirmed by COMSOL simulations carried out for the $s_y = 0.52$ μm structure chosen because $|q_{xx}| \approx |q_{yy}|$ according to Fig. 3(b). The peak enhancement factor $\eta_{\max}(\phi) \equiv \eta(\lambda'_Q, \phi)$ plotted in Fig. 3(b) reveals strong CD. The ratio of the highest ($\phi_{\max} \approx 210°$) to lowest ($\phi_{\min} \approx 30°$) near-field intensities is ≈20, and the enhancement ratio for right-hand circularly polarized light ($\phi = -90°$) is ≈3 times higher than for the left-hand circularly polarized light ($\phi = 90°$).

Because $\eta_{\max}(\phi)$ and peak Ohmic loss $A(\phi)$ are proportional to each other, ϕ emerges as a powerful tool for controlling the absorption using the interference of the polarization components of elliptically polarized light. For example, we find for the DCF metasurface shown in Fig. 3(b) that $A(\phi_{\min}) \approx 1.5\%$, i.e., the absorption is coherently suppressed. On the other hand, $A(\phi_{\max}) \approx 41\%$, i.e., the absorption is coherently enhanced almost to the absolute absorption limit ($A_{\lim} = 50\%$) of a thin layer in vacuum [24]. Another important consequence of the related giant CD absorbance of the DCF metasurface ($A_{\mathrm{RCP}} = 30\%$ versus $A_{\mathrm{LCP}} = 13\%$) is that it exhibits circular conversion dichroism [18] due to the dissipation asymmetry between right-hand circularly polarized and left-hand circularly polarized light.

In conclusion, we have demonstrated that a quantum mechanical phenomenon of double continuum Fano interference can be classically emulated using an asymmetric plasmonic metasurface. The relative coupling strength between the discrete and two continuum states, distinguished from each other by their polarization, were experimentally varied by changing the degree of symmetry

breaking of the metasurface. The phenomenon of continuum state competition, by which one of the continuum states suppresses the Fano resonance for the orthogonal light polarization, was observed and analytically explained. This work opens new possibilities for controlling optical energy concentration on the nanoscale using the ellipticity state of the incident light, thereby providing a simple and powerful tool for developing novel nanophotonic applications such as sensors and detectors.

This work was supported by the Office of Naval Research (ONR) Grant No. N00014-13-1-0837 and by the National Science Foundation (NSF) Grant No. DMR 1120923.

*gena@physics.utexas.edu

[1] U. Fano, Phys. Rev. **124**, 1866 (1961).
[2] S. Fan and J. D. Joannopoulos, Phys. Rev. B **65**, 235112 (2002).
[3] V. A. Fedotov, M. Rose, S. L. Prosvirnin, N. Papasimakis, and N. I. Zheludev, Phys. Rev. Lett. **99**, 147401 (2007).
[4] A. E. Miroshnichenko, S. Flach, and Y. S. Kivshar, Rev. Mod. Phys. **82**, 2257 (2010).
[5] B. Luk'yanchuk, N. I. Zheludev, S. A. Maier, N. J. Halas, P. Nordlander, H. Giessen, and C. T. Chong, Nat. Mater. **9**, 707 (2010).
[6] N. Liu, L. Langguth, T. Weiss, J. Kastel, M. Fleischhauer, T. Pfau, and H. Giessen, Nat. Mater. **8**, 758 (2009).
[7] C. Wu, A. B. Khanikaev, R. Adato, N. Arju, A. A. Yanik, H. Altug, and G. Shvets, Nat. Mater. **11**, 69 (2012).
[8] F. Hao, Y. Sonnefraud, P. Van Dorpe, S. A. Maier, N. J. Halas, and P. Nordlander, Nano Lett. **8**, 3983 (2008).
[9] C.-Y. Chao and L. J. Guo, Appl. Phys. Lett. **83**, 1527 (2003).
[10] N. Liu, M. L. Tang, M. Hentschel, and H. Giessen, Nat. Mater. **10**, 631 (2011).
[11] J. B. Pendry, A. J. Holden, D. J. Robbins, and W. J. Stewart, IEEE Trans. Microwave Theory Tech. **47**, 2075 (1999).
[12] R. S. Benninnk, Y.-K. Yoon, R. W. Boyd, and J. E. Sipe, Opt. Lett. **24**, 1416 (1999).
[13] A. B. Khanikaev, C. Wu, and G. Shvets, Nanophotonics **2**, 247 (2013).
[14] B. Gallinet and O. J. F. Martin, Phys. Rev. B **83**, 235427 (2011).
[15] C. Wu, A. B. Khanikaev, and G. Shvets, Phys. Rev. Lett. **106**, 107403 (2011).
[16] E. J. Osley, C. G. Biris, P. G. Thompson, R. R. F. Jahromi, P. A. Warburton, and N. C. Panoiu, Phys. Rev. Lett. **110**, 087402 (2013).
[17] Y. D. Chong, L. Ge, H. Cao, and A. D. Stone, Phys. Rev. Lett. **105**, 053901 (2010).
[18] V. A. Fedotov, P. L. Mladyonov, S. L. Prosvirnin, A. V. Rogacheva, Y. Chen, and N. I. Zheludev, Phys. Rev. Lett. **97**, 167401 (2006).
[19] H. Haus, *Waves and Fields in Optoelectronics* (Prentice-Hall, Englewood Cliffs, NJ, 1984).
[20] S. Fan, W. Suh, and J. D. Joannopoulos, J. Opt. Soc. Am. A **20**, 569 (2003).
[21] See Supplemental Material at http://link.aps.org/supplemental/10.1103/PhysRevLett.114.237403, which includes Refs. [22] and [23], for details of the analytic calculation and numerical extraction of the coupling coefficients.
[22] J. C. Slater, Rev. Mod. Phys. **18**, 441 (1946).
[23] G. E. Dombrowski, J. Appl. Phys. **55**, 2648 (1984).
[24] F. J. Garca de Abajo, Rev. Mod. Phys. **79**, 1267 (2007).